

**Electronic Supplementary Information**

**Porphyrin-based mixed-valent Ag(I)/Ag(II) and Cu(I)/Cu(II) networks as efficiently heterogeneous catalysts for azide–alkyne “Click” reaction and promising oxidation of ethylbenzene**

**Wei Jiang, Jin Yang,\* Ying-Ying Liu and Jian-Fang Ma\***

*Key Lab for Polyoxometalate Science, Department of Chemistry, Northeast Normal University, Changchun 130024, People’s Republic of China*

\* Correspondence authors

E-mail: yangj808@nenu.edu.cn (J. Yang)

Fax: +86-431-85098620 (J.-F. Ma)

E-mail: majf247@yahoo.com (J.-F. Ma)

## Experimental section

**Materials and general methods.** All reagents and solvents were purchased from commercial sources and used without further purification. Elemental analyses were conducted by a Perkin-Elmer 240CHN elemental analyzer. FT-IR spectra were measured from KBr pellets in the 4000–400  $\text{cm}^{-1}$  range on a Mattson Alpha-Centauri spectrometer. PXRD patterns were recorded on a Rigaku Dmax 2000 X-ray diffractometer with graphite monochromatized Cu  $K\alpha$  radiation ( $\lambda = 0.154 \text{ nm}$ ) and  $2\theta$  ranging from 5 to 30°.  $^1\text{H}$  NMR spectra were recorded on a Varian 500 MHz.  $^{13}\text{C}$  NMR spectra were recorded on a Varian 125 MHz. Thermogravimetric (TG) measurements were performed on a Perkin-Elmer TG-7 analyzer from 30 to 1000 °C at a rate of 5 °C  $\text{min}^{-1}$  under nitrogen gas. The catalytic products were measured by gas chromatograph equipment with capillary (30 m long  $\times$  0.25 mm i.d., WondaCAP 17), and FID detector (GC-2014C, Shimadzu, Japan). UV-vis spectra were measured on a TU-1900 UV-Vis spectrophotometer (Beijing Purkinje General Instrument Co. Ltd., China).

**Visible photocatalytic reduction of Cr(VI).** The experiments were carried out through a conventional process in aqueous solution. Typically, 50 mg of crystals and 20 mL of isopropanol were added into  $\text{K}_2\text{Cr}_7\text{O}_7$  aqueous solution. The solution was stirred in the dark for 30 minutes to guarantee adsorption-desorption equilibrium. Then, the mixture was stirred under the irradiation of Xe lamp, which was used as the visible light source with a cutoff filter. At 15 min intervals, a series of 3 mL sample solutions were taken out from the reaction system and separated by centrifugation to give the supernatant liquid without catalyst particles. During the reduction process, the separated sample was monitored by UV-vis spectrophotometer.

**Azide–alkyne cycloaddition reactions.** In a typical procedure, benzyl chloride (1 mmol, 126 mg), phenylacetylene (2 mmol, 204 mg), sodium azide (1.2 mmol, 78 mg) and amyl acetate as internal standard (0.92 mmol, 120 mg) were dissolved in methanol/water (5 mL, 4:1). Then the catalyst (0.01 mmol, 25 mg) was added into the solution and the mixture was heated at 50 °C for 12 h. The structure of the product

was confirmed by  $^1\text{H}$  NMR and single-crystal X-ray diffraction. The yields of the products were calculated by GC based on the content of phenylacetylene.  $^1\text{H}$  NMR (500 MHz,  $[\text{D}_6]$  DMSO, TMS) for 1-benzyl-4-phenyl-1H-1,2,3-triazole (**2a**):  $\delta$  5.57 (s, 2H), 7.27-7.44 (m, 8H), 7.76-7.84 (s, 2H), 7.68 (s, 1H); 1-(4-fluoro-benzyl)-4-phenyl-1H-1,2,3-triazole (**2b**):  $\delta$  5.85 (s, 2H), 7.21-7.44 (m, 8H), 7.85-7.87 (s, 2H); 1-(4-methyl-benzyl)-4-phenyl-1H-1,2,3-triazole (**2c**):  $\delta$  2.21-2.34 (s, 3H), 5.54-5.65 (s, 2H), 7.10-7.57 (m, 8H), 7.78-7.95 (s, 2H); 1-(3-methyl-benzyl)-4-phenyl-1H-1,2,3-triazole (**2d**):  $\delta$  2.26-2.30 (s, 3H), 5.63 (s, 2H), 7.15-7.44 (m, 8H), 7.84-7.86 (s, 2H).  $^{13}\text{C}$  NMR (125 MHz,  $[\text{D}_1]$  chloroform, TMS) for 1-benzyl-4-phenyl-1H-1,2,3-triazole (**2a**):  $\delta$  54.0, 119.3, 125.6, 128.1, 128.7, 129.7, 130.5, 131.5, 131.6, 138.7, 148.1; 1-(4-fluoro-benzyl)-4-phenyl-1H-1,2,3-triazole (**2b**):  $\delta$  47.6, 115.7, 124.8, 125.6, 128.1, 128.7, 129.1, 120.5, 130.8, 148.2, 159.5, 161.4; 1-(4-methyl-benzyl)-4-phenyl-1H-1,2,3-triazole (**2c**):  $\delta$  21.1, 54.0, 125.6, 128.1, 128.7, 129.7, 130.5, 131.6, 138.7, 148.1; 1-(3-methyl-benzyl)-4-phenyl-1H-1,2,3-triazole (**2d**):  $\delta$  21.6, 53.6, 125.8, 126.0, 127.7, 128.7, 129.7, 131.3, 132.1, 133.1, 136.5, 138.9, 147.6.

**Oxidation of ethylbenzene.** A mixture of catalyst **1** (25 mmol, 6 mg), ethylbenzene (25 mmol, 26 mg), TBHP (1 mmol, 128 mg) and amyl acetate as internal standard (20 mmol, 26 mg) in water (4 mL) was stirred at 50 °C for 12 h. The mixture was centrifugated and subsequently extracted with  $\text{CH}_2\text{Cl}_2$ . The oxidation products were confirmed by comparison with GC signal of the commercial acetophenone. The yields were calculated by GC. Quenching experiment of radicals was carried out in the presence of *p*-benzoquinone (5 mmol, 5.4 mg).

**Synthesis of  $[\text{Cu}(\text{I})_6\text{I}_6(\text{Cu}(\text{II})\text{-TPPP})]\cdot 2\text{DMF}$  (**1**).** A mixture of  $\text{H}_2\text{TPPP}$  (20 mg, 0.017 mmol), CuI (100 mg, 0.525 mmol) and DMF (8 mL) was placed in a Teflon reactor (15 mL) and heated at 130 °C for 72 h, and then was gradually cooled to room temperature at a rate of 10 °C $\cdot$ h $^{-1}$ . The dark purple crystals of **1** were obtained in a 50% yield. Anal. Calcd for  $\text{C}_{78}\text{H}_{58}\text{N}_{22}\text{O}_2\text{I}_6\text{Cu}_7$ : C, 36.86%; H, 2.30%; N, 12.12%. Found: C, 36.65%; H, 2.11%; N, 12.29%. IR (KBr pellet,  $\text{cm}^{-1}$ ): 3421(m), 1669(m), 1506(s), 1484(m), 1406(s), 1383(m), 1361(s), 1344(m), 1312(w), 1270(m), 1167(w), 1152(w),

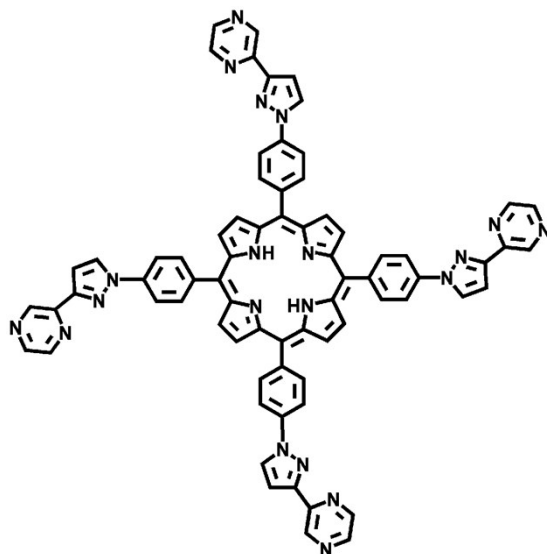
1058(w), 998(s), 964(w), 945(m), 807(m), 767(m).

**Synthesis of [Ag(I)(NO<sub>3</sub>)<sub>0.5</sub>(Ag(II)-TPPP)]·0.5NO<sub>3</sub>·DMF (2).** A mixture of H<sub>2</sub>TPPP (20 mg, 0.017 mmol), AgNO<sub>3</sub> (30 mg, 176 mmol) and DMF (8 mL) was placed in a Teflon reactor and heated at 100 °C for 72 h, and then it was gradually cooled to room temperature at a rate of 10 °C·h<sup>-1</sup>. The dark purple crystals of **2** were achieved in a 31% yield. Anal. Calcd for C<sub>75</sub>H<sub>51</sub>N<sub>22</sub>O<sub>4</sub>Ag<sub>2</sub>: C, 58.49%; H, 3.34%; N, 20.00%. Found: C, 58.81%; H, 3.52%; N, 20.39%. IR (KBr pellet, cm<sup>-1</sup>): 3419(w), 1668(m), 1517(s), 1482(m), 1459(w), 1404(m), 1382(s), 1361(s), 1337(s), 1314(m), 1268(s), 1150(m), 1124(w), 1055(s), 1004(s), 962(m), 944(s), 852(w), 807(m), 788(m), 767(m).

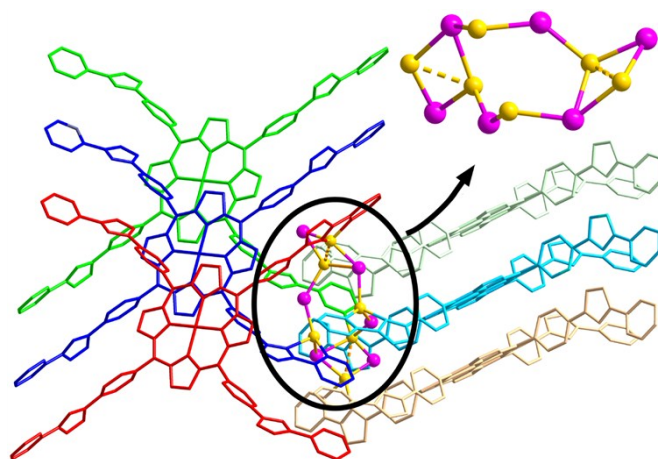
**X-ray crystallography.** Single-crystal X-ray diffraction data of **1** and **2** were recorded on an Oxford Diffraction Gemini R CCD diffractometer with graphite-monochromated Mo K $\alpha$  radiation ( $\lambda = 0.71073$  Å) at 293 K. All absorption corrections were applied using a multi-scan technique. The structures were solved by direct methods and refined on F<sup>2</sup> full-matrix least-squares using the SHELXTL-97 program within WINGX.<sup>1</sup> All non-hydrogen atoms were refined anisotropically. The carbon hydrogen atoms were generated geometrically. Because of the presence of voids of about 11% of the crystal volume in **2**, we tried to locate some solvents from the difference Fourier maps, however, not any suitable diffraction peaks were found. Selected bond distances and angles are given in Tables S4 and S5. Crystallographic data of the compounds are listed in Tables S6 and S7.

## References

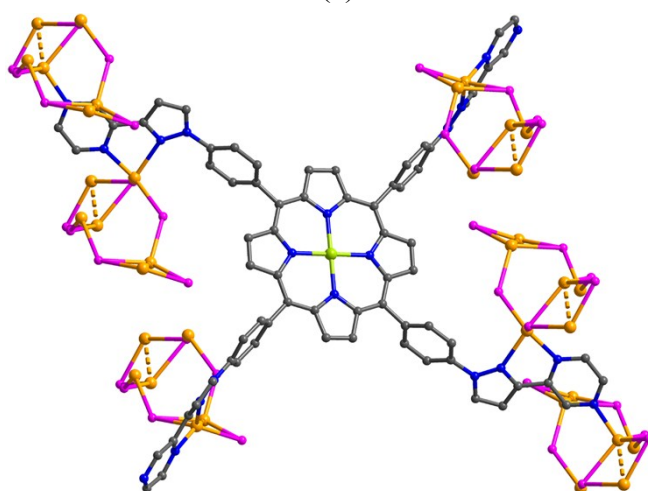
- (1) (a) G. M. Sheldrick, SHELXL-97, *Programs for X-ray Crystal Structure Solution*; University of Göttingen: Göttingen, Germany, 1997; (b) G. M. Sheldrick, SHELXL-97, *Programs for X-ray Crystal Structure Refinement*; University of Göttingen: Göttingen, Germany, 1997; (c) L. J. Farrugia, WINGX: *A Windows Program for Crystal Structure Analysis*; University of Glasgow: Glasgow, UK, 1988.



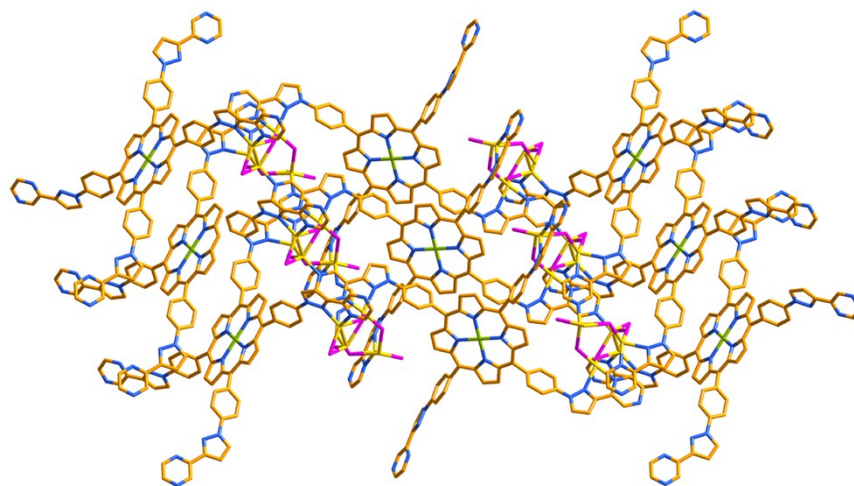
**Scheme S1.** Chemical structure of H<sub>2</sub>TPPP.



(a)

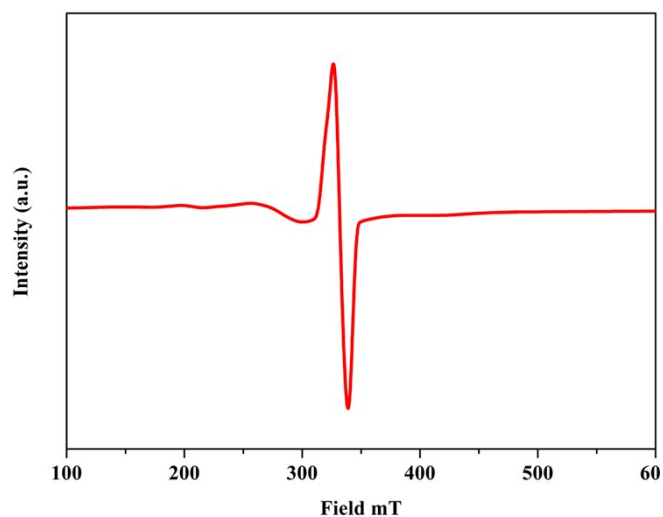


(b)

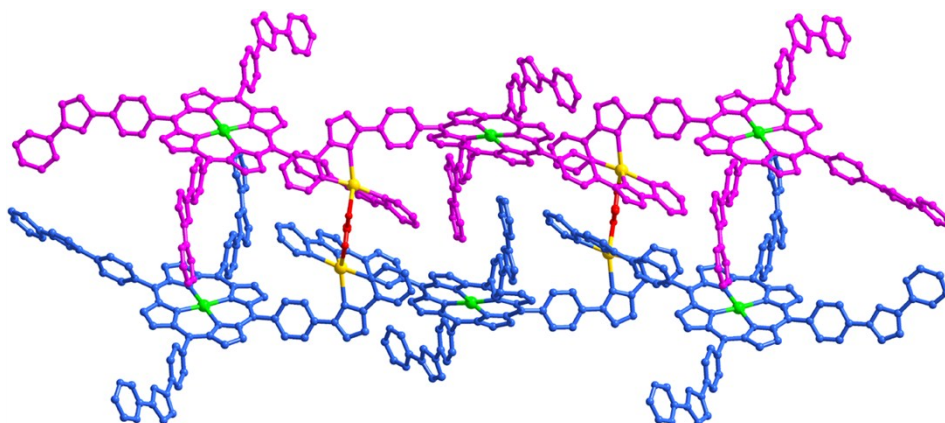


(c)

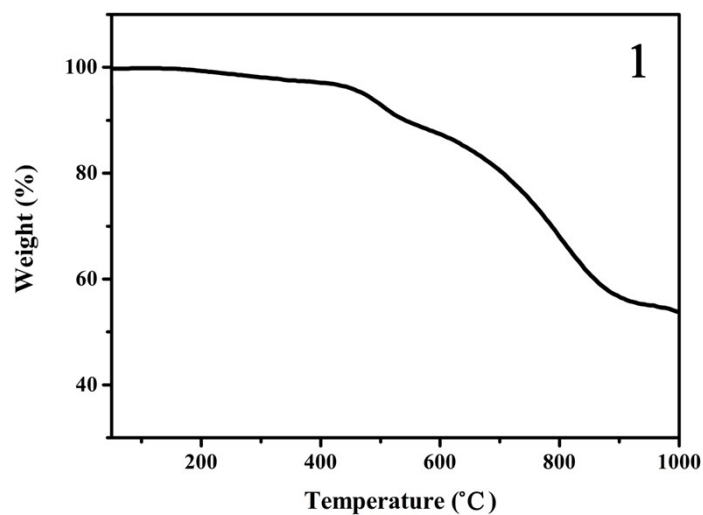
**Fig. S1.** (a) Coordination modes of  $[\text{Cu}_6\text{I}_6]$  cluster. (b) Coordination modes of  $\text{Cu(II)}$ -TPPP in **1**. (c) View of the 2D network of **1**.



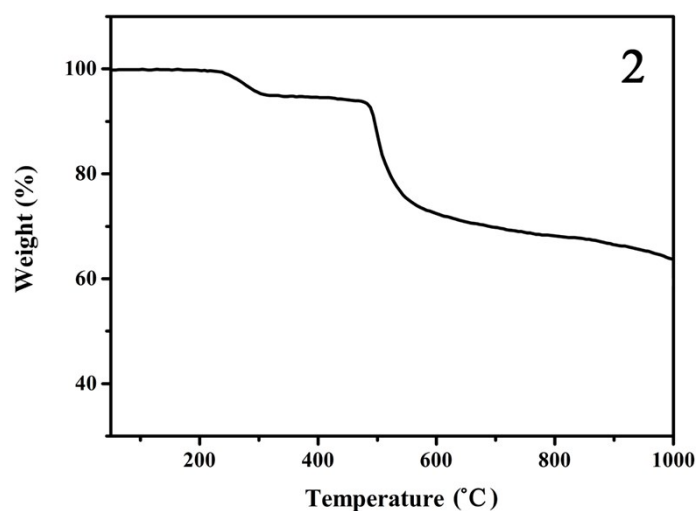
**Fig. S2.** The electron paramagnetic resonance (EPR) spectrum of **2**.



**Fig. S3.** View of the 1D double-chain of **2**.



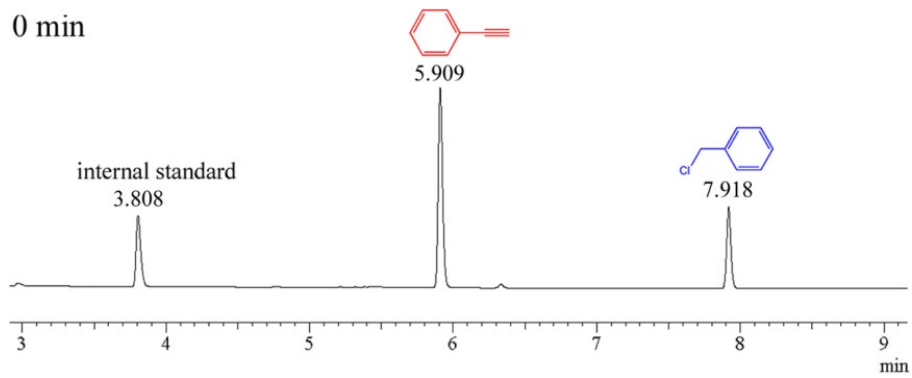
(a)



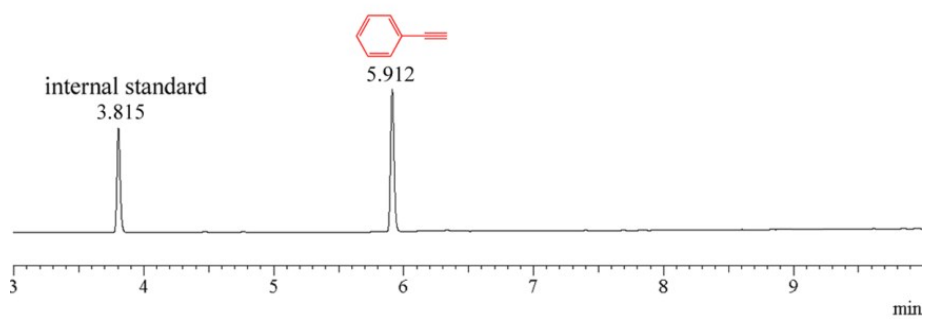
(b)

**Fig. S4.** Thermogravimetric curves of **1** (a) and **2** (b).

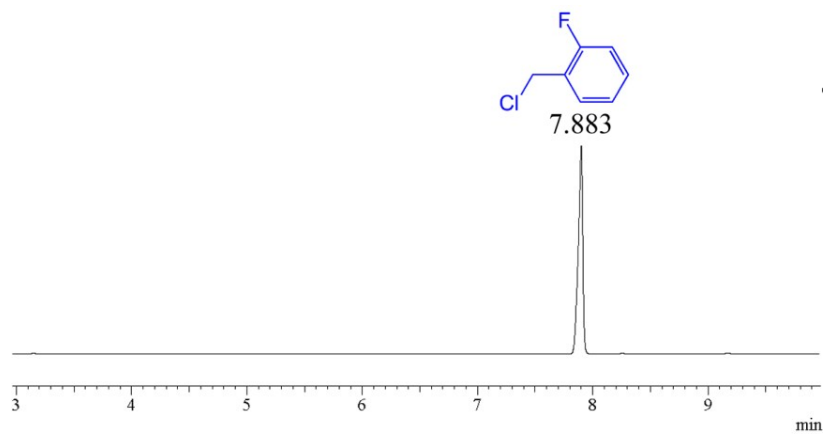
Thermogravimetric analyses were performed under nitrogen gas from 30 to 1000 °C. For **1**, the weight loss in the temperature range of 192-422 °C corresponds to the removal of DMF molecules (obsd 4.8 %, calcd 5.7%). From 422 to 1000 °C, the weight loss is probably attributed to the decomposition of the network. For **2**, the lose weight in the temperature range of 223-318°C corresponds to the removal of DMF molecules (obsd 4.9 %, calcd 4.7%). The network begins to decompose from 473°C.



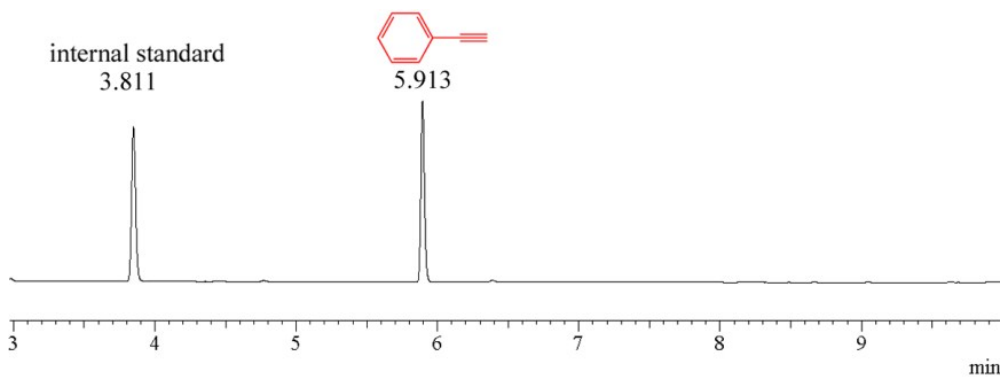
(a)



(b)

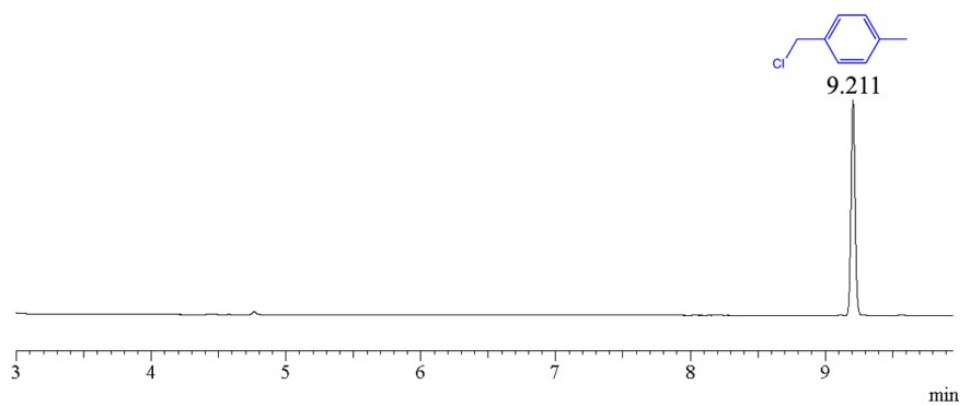


(c)

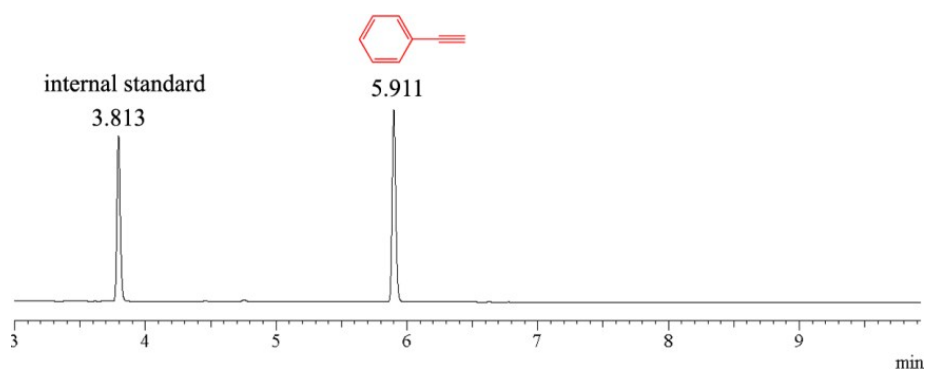


(d)

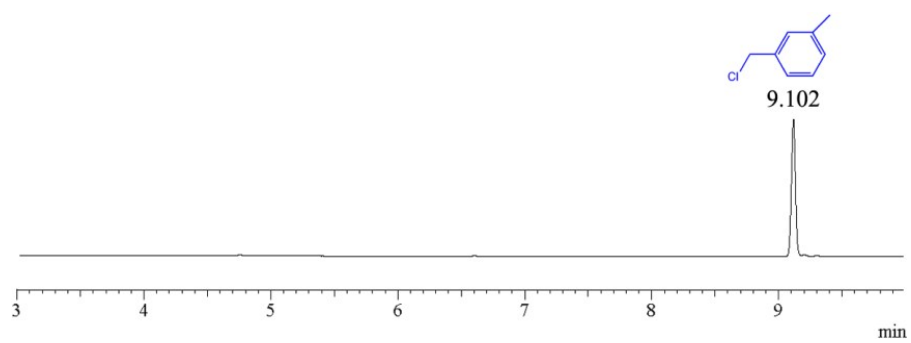




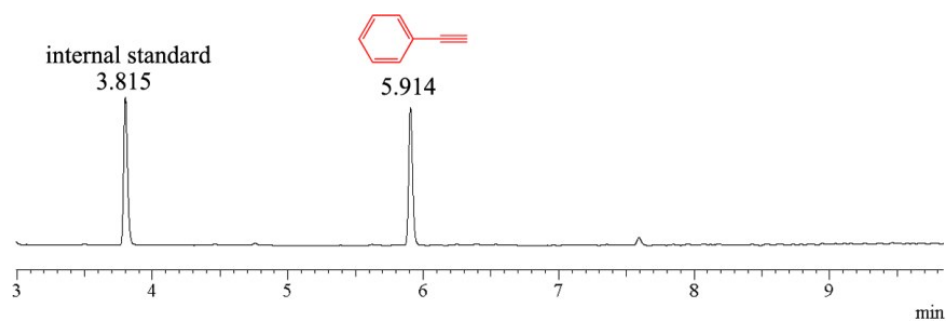
(e)



(f)



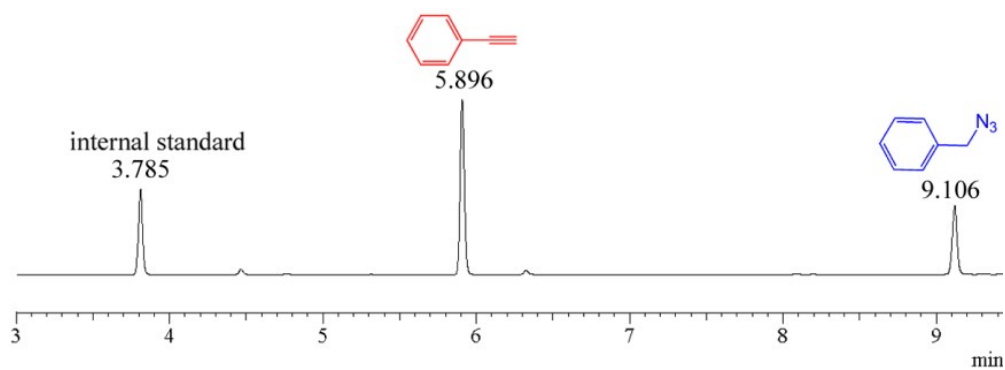
(g)



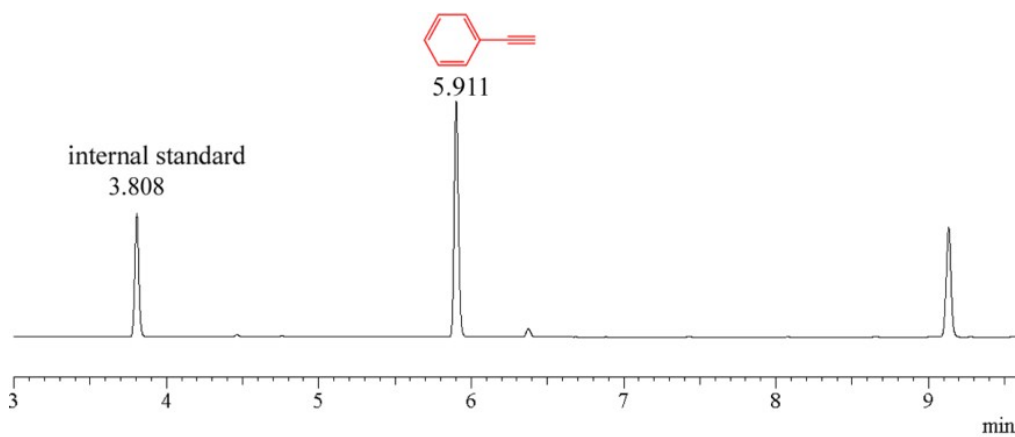
(h)

**Fig. S5.** (a) GC of the blank experiment using internal standard, phenylacetylene and benzyl chloride. (b) GC of the AAC experiment using benzyl chloride,

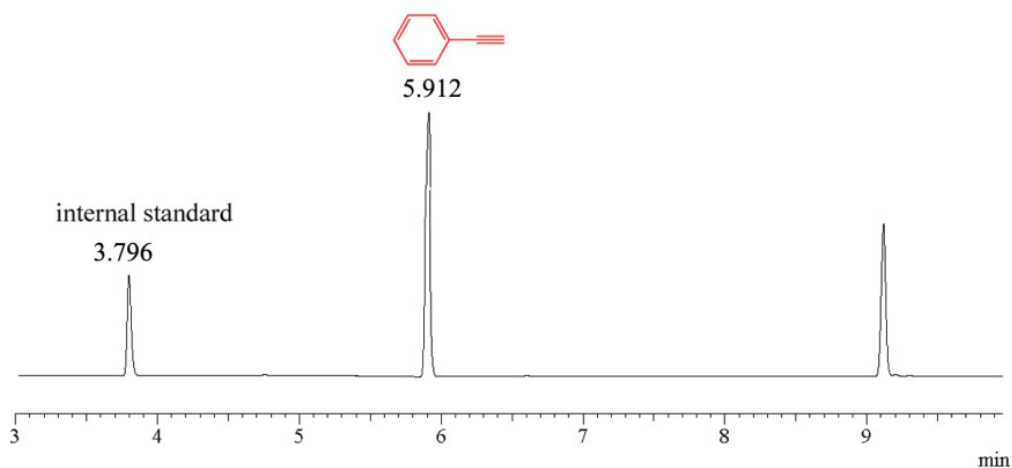
phenylacetylene, catalyst **1** and internal standard. (c) GC of the blank experiment of 2-fluorobenzyl chloride. (d) GC of the AAC experiment using 2-fluorobenzyl chloride, phenylacetylene, catalyst **1** and internal standard. (e) GC of the blank experiment using 4-methylbenzyl chloride. (f) GC of the AAC experiment using 4-methylbenzyl chloride, phenylacetylene, catalyst **1** and internal standard. (g) GC of the blank experiment using 3-methylbenzyl chloride. (h) GC of the AAC experiment using 3-methylbenzyl chloride, phenylacetylene, catalyst **1** and internal standard.



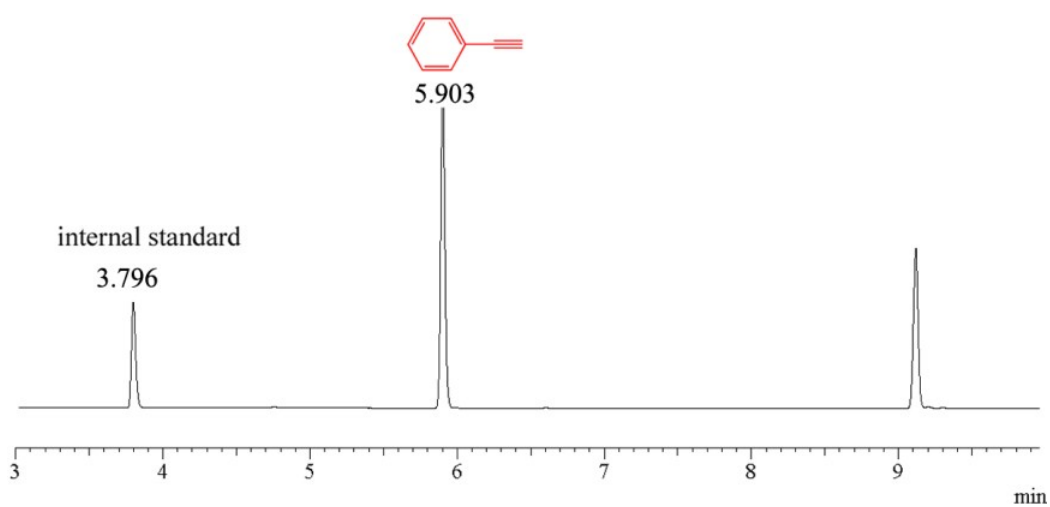
(a)



(b)



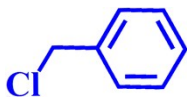
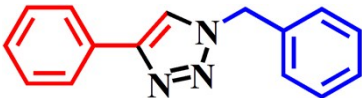
(c)


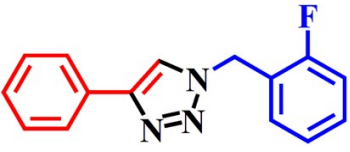
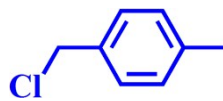
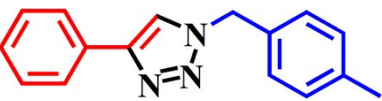
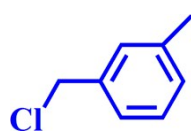
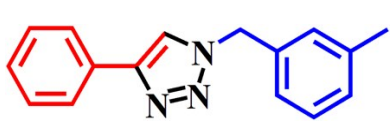



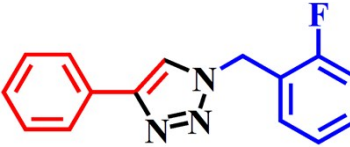
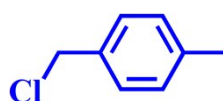
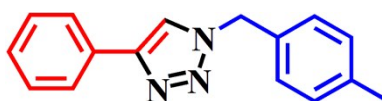
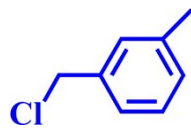
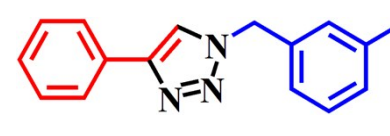


(d)

**Fig. S6.** (a) GC of the AAC experiment using benzyl chloride, phenylacetylene, catalyst **2** and internal standard. (b) GC of the AAC experiment using 2-fluorobenzyl chloride, phenylacetylene, catalyst **2** and internal standard. (c) GC of the AAC experiment using 4-methylbenzyl chloride, phenylacetylene, catalyst **2** and internal standard. (d) GC of the AAC experiment using 3-methylbenzyl chloride phenylacetylene, catalyst **2** and internal standard.

**Table S1.** Catalytic activities of **1** and **2** in the AAC reactions<sup>a</sup>

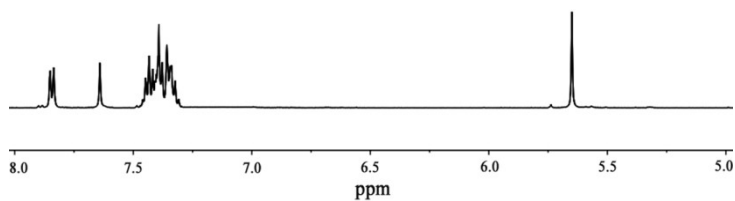
Entry	Chloride	Product	Catalyst	Yield <sup>b</sup>
1			<b>1</b>	>99%

2	<p><b>1a</b></p> 	<p><b>2a</b></p> 	<b>1</b>	>99%
3	<p><b>1b</b></p> 	<p><b>2b</b></p> 	<b>1</b>	>99%
4	<p><b>1c</b></p> 	<p><b>2c</b></p> 	<b>1</b>	>99%
5	<p><b>1d</b></p> 	<p><b>2d</b></p> 	<b>2</b>	40%
6	<p><b>1a</b></p> 	<p><b>2a</b></p> 	<b>2</b>	42%
7	<p><b>1b</b></p> 	<p><b>2b</b></p> 	<b>2</b>	trace
8	<p><b>1c</b></p> 	<p><b>2c</b></p> 	<b>2</b>	trace

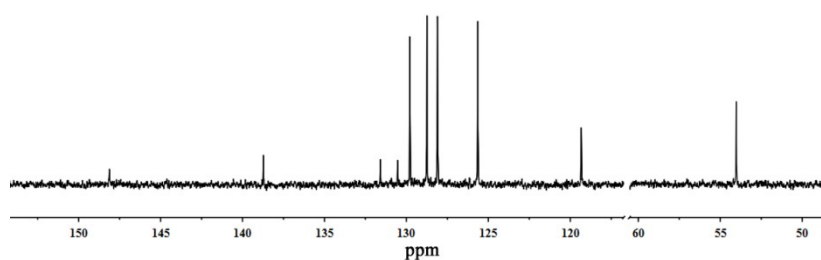
<sup>a</sup>Reaction conditions: phenylacetylene (2 mmol), benzyl chloride (1 mmol), sodium azide (1.2 mmol), catalyst (1 mol %), methanol (4 mL), water (1 mL), 50 °C, 12 h.

<sup>b</sup>Isolated yield was calculated by GC.

**1-benzyl-4-phenyl-1H-1,2,3-triazole 2a:**

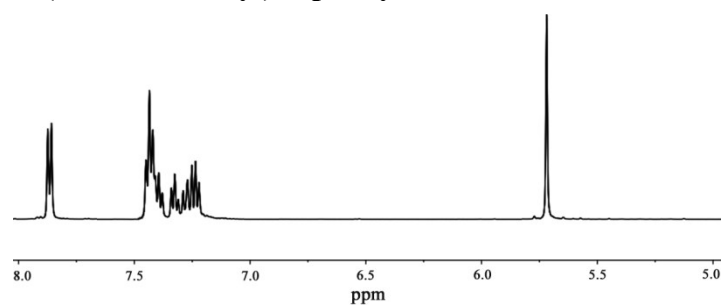


(a)

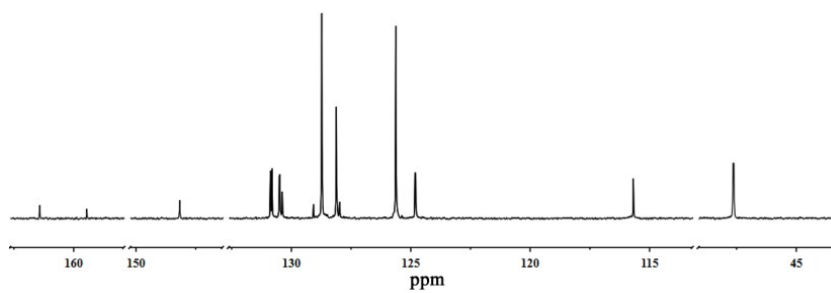


(b)

**1-(2-fluoro-benzyl)-4-phenyl-1H-1,2,3-triazole 2b:**

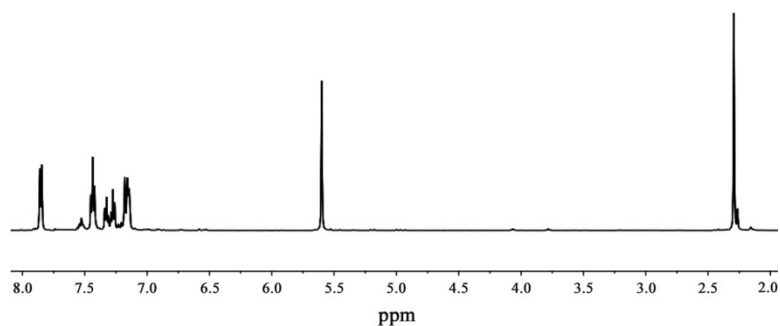


(c)

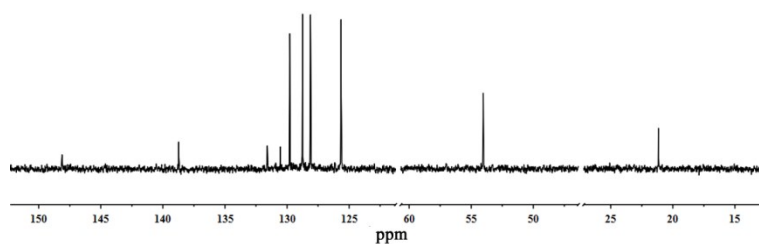


(d)

**1-(4-methyl-benzyl)-4-phenyl-1H-1,2,3-triazole 2c:**

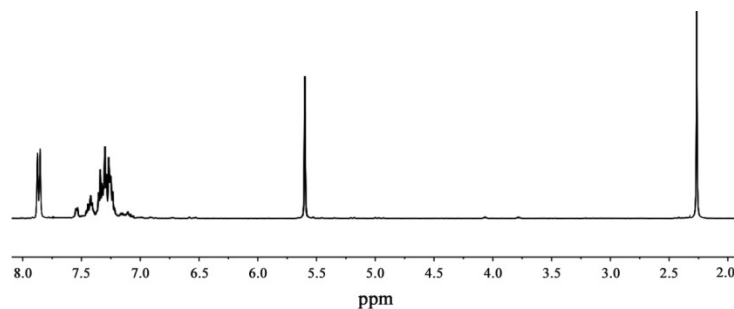


(e)

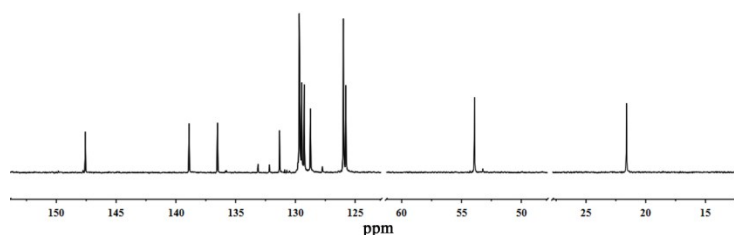


(f)

**1-(3-methyl-benzyl)-4-phenyl-1H-1,2,3-triazole 2d:**

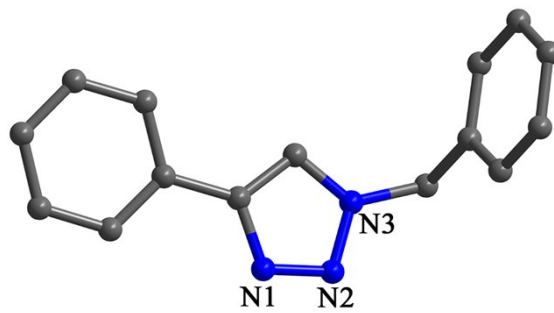


(g)

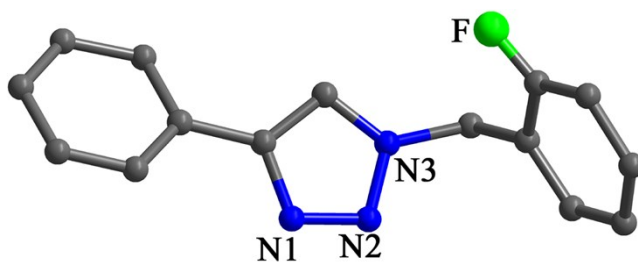


(h)

**Fig. S7.** (a)  $^1\text{H}$  NMR spectrum of 1-benzyl-4-phenyl-1H-1,2,3-triazole **2a**. (b)  $^{13}\text{C}$  NMR spectrum of 1-benzyl-4-phenyl-1H-1,2,3-triazole **2a**. (c)  $^1\text{H}$  NMR spectrum of 1-(2-fluoro-benzyl)-4-phenyl-1H-1,2,3-triazole **2b**. (d)  $^{13}\text{C}$  NMR spectrum of 1-(2-fluoro-benzyl)-4-phenyl-1H-1,2,3-triazole **2b**. (e)  $^1\text{H}$  NMR spectrum of 1-(4-methyl-benzyl)-4-phenyl-1H-1,2,3-triazole **2c**. (f)  $^{13}\text{C}$  NMR spectrum of 1-(4-methyl-benzyl)-4-phenyl-1H-1,2,3-triazole **2c**. (g)  $^1\text{H}$  NMR spectrum of 1-(3-methyl-benzyl)-4-phenyl-1H-1,2,3-triazole **2d**. (h)  $^{13}\text{C}$  NMR spectrum of 1-(3-methyl-benzyl)-4-phenyl-1H-1,2,3-triazole **2d**.

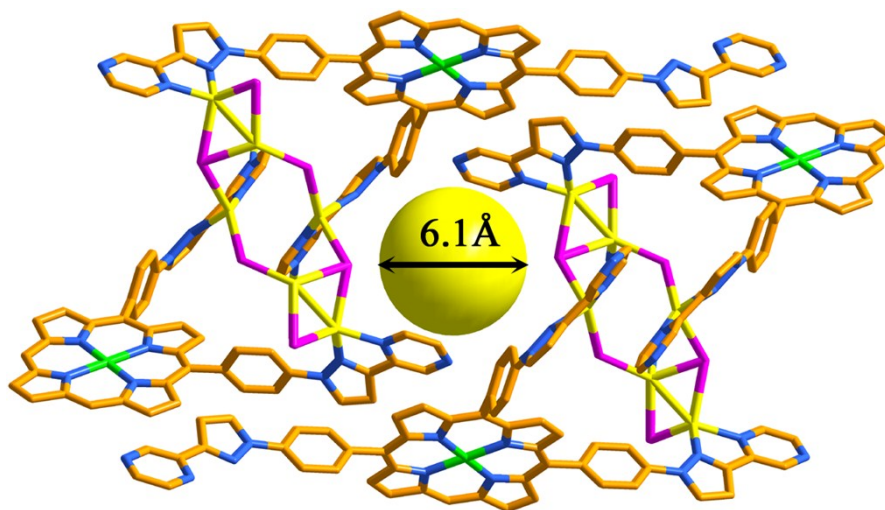


(a)

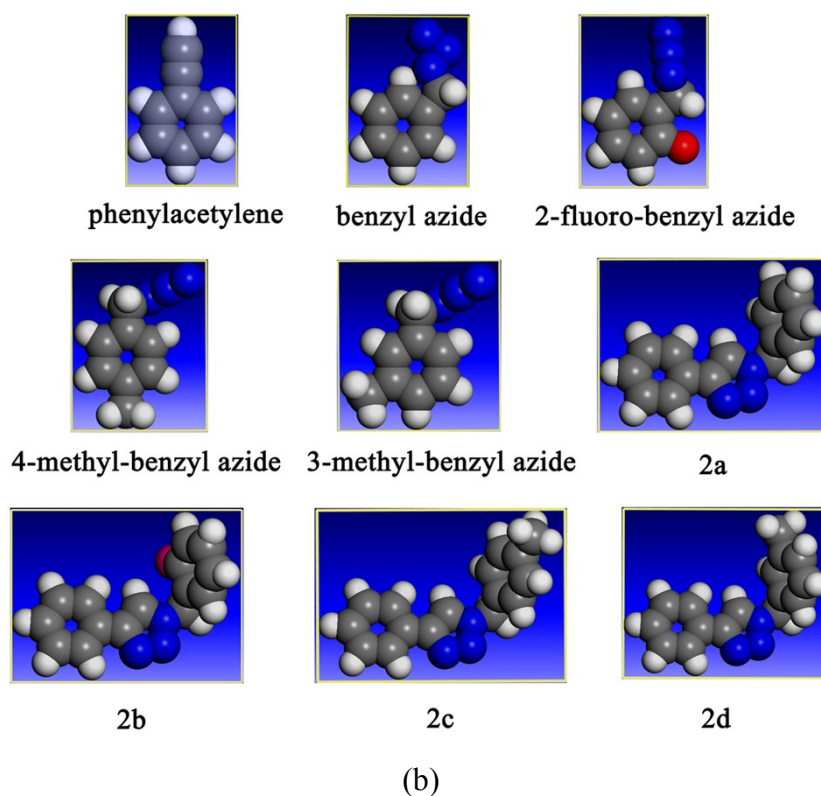


(b)

**Fig. S8.** Crystal structures of 1-benzyl-4-phenyl-1H-1,2,3-triazole **2a** (a) and 1-(2-fluoro-benzyl)-4-phenyl-1H-1,2,3-triazole **2b** (b).



(a)

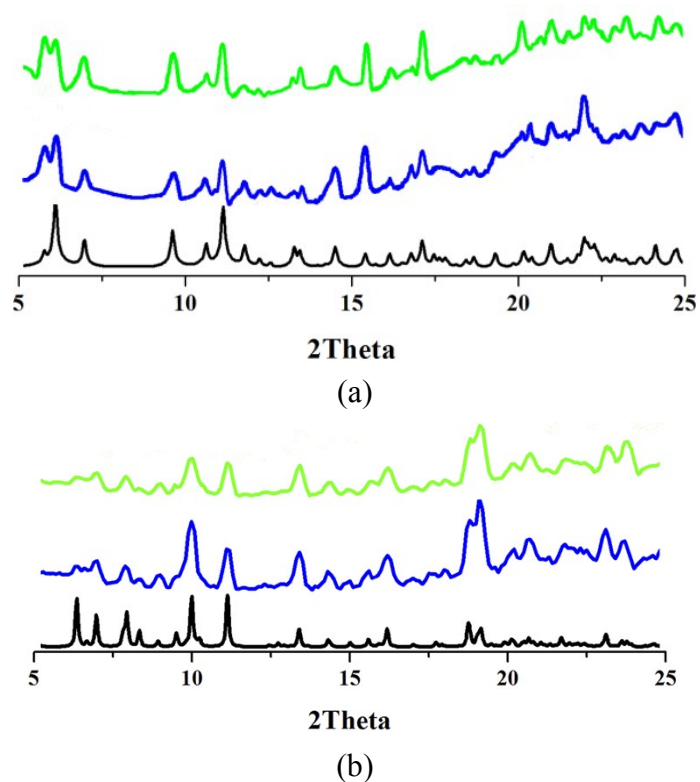


**Fig. S9.** (a) View of the cavity diameter of **1**. (b) Chemical structures of the starting materials and products used in the AAC reactions.

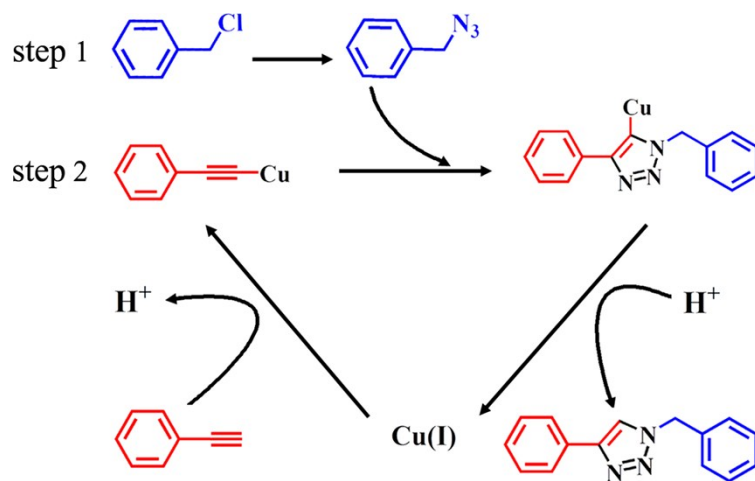
**Table S2.** Molecular dimensions of the starting materials and products used in the AAC reactions

	$x$ (Å)	$y$ (Å)	$z$ (Å)
phenylacetylene	6.0	9.3	2.5
2-fluoro-benzyl azide	7.6	10.3	3.6
4-methyl-benzyl azide	8.0	10.1	4.1
3-methyl-benzyl azide	9.0	9.5	4.2
<b>2a</b>	13.5	10.1	6.6
<b>2b</b>	13.5	10.1	6.6
<b>2c</b>	15.4	10.7	7.0
<b>2d</b>	13.6	11.1	6.8

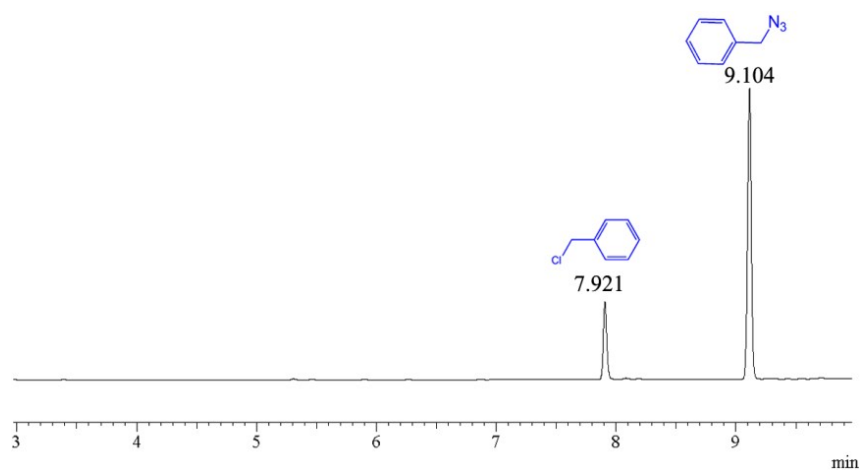




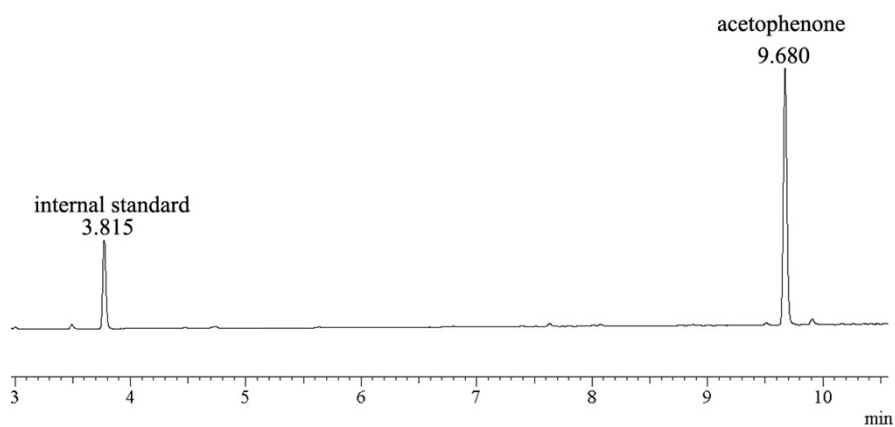
**Fig. S10.** (a) PXRD patterns of the simulated (black), the experimental (blue) and the AAC catalyzed by **1** (green). (b) PXRD patterns of the simulated (black), the experimental (blue) and the AAC catalyzed by **2** (green).



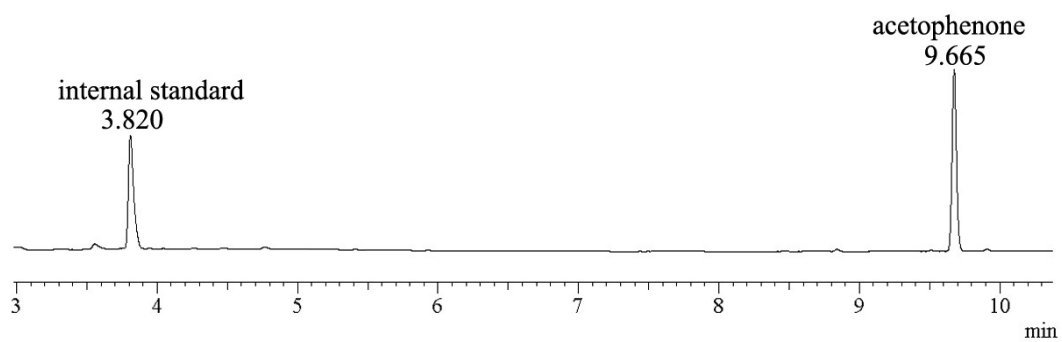
**Scheme S2.** Proposed mechanism of the AAC reaction in a “one-pot two-step domino” way by using catalyst **1**.



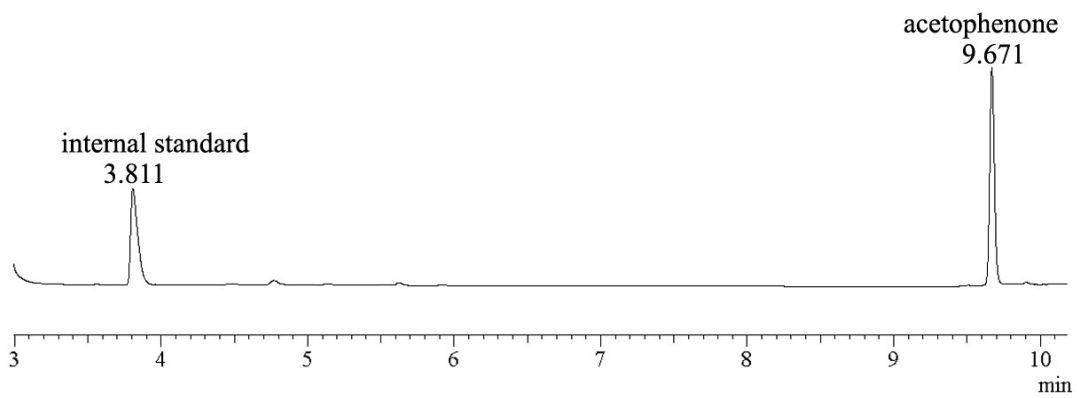
**Fig. S11.** GC of the reaction of benzyl chloride with sodium azide.



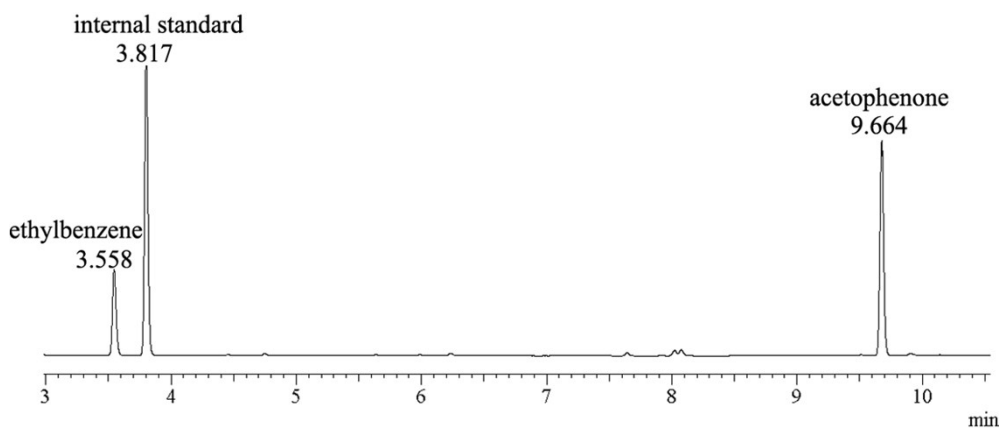
(a)



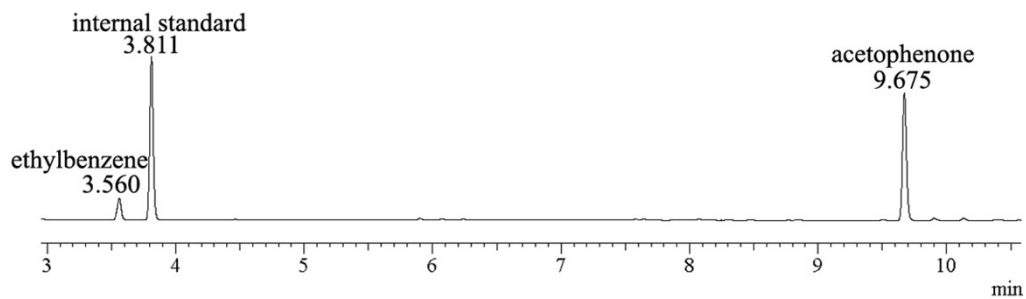
(b)



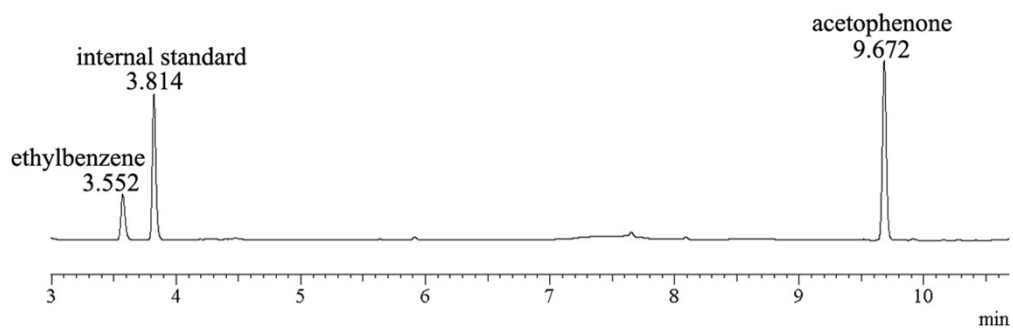
(c)



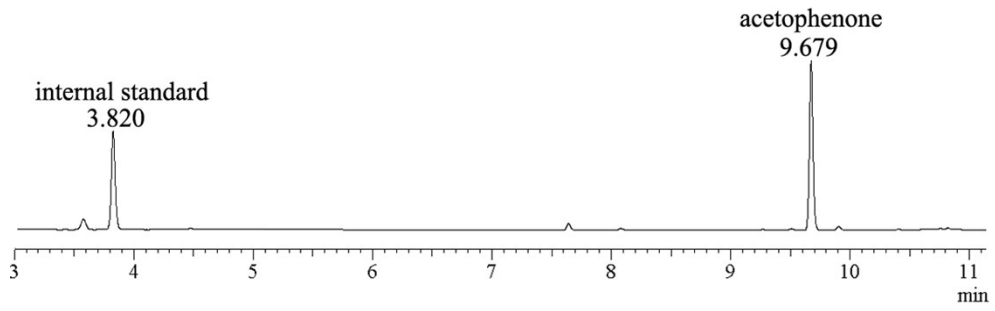
(d)



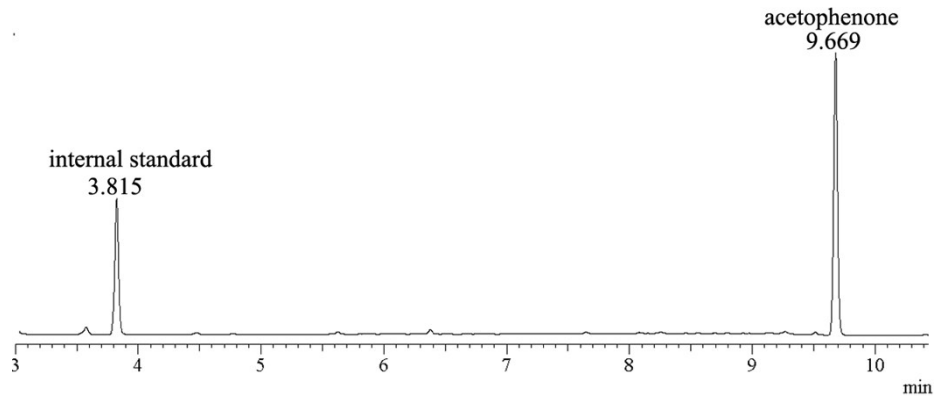
(e)



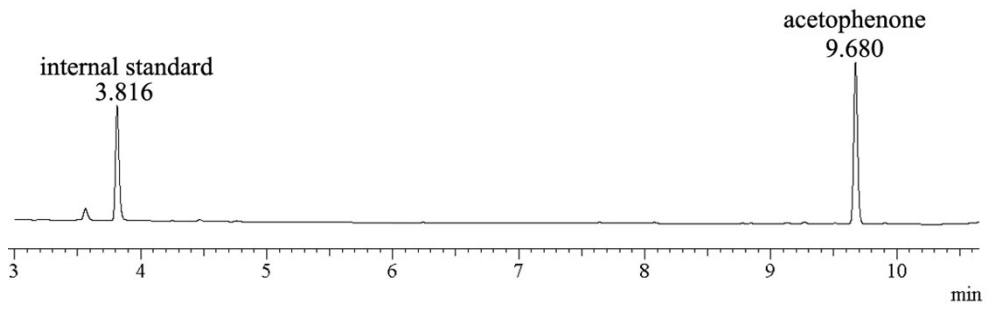
(f)



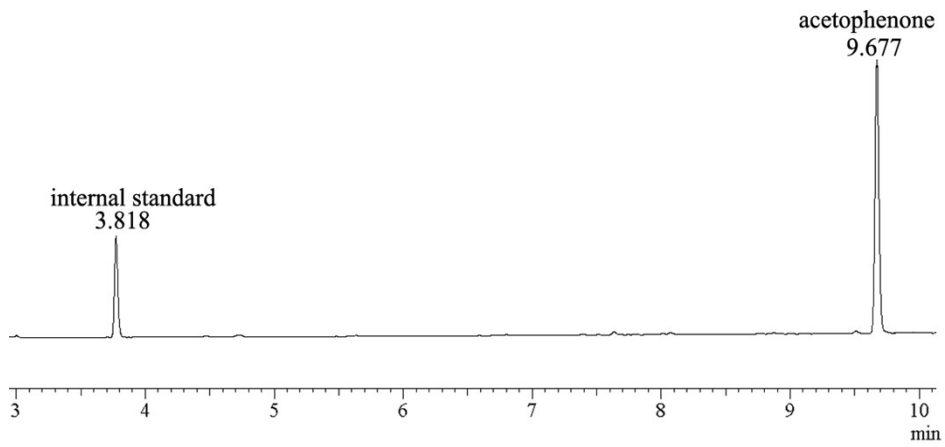
(g)



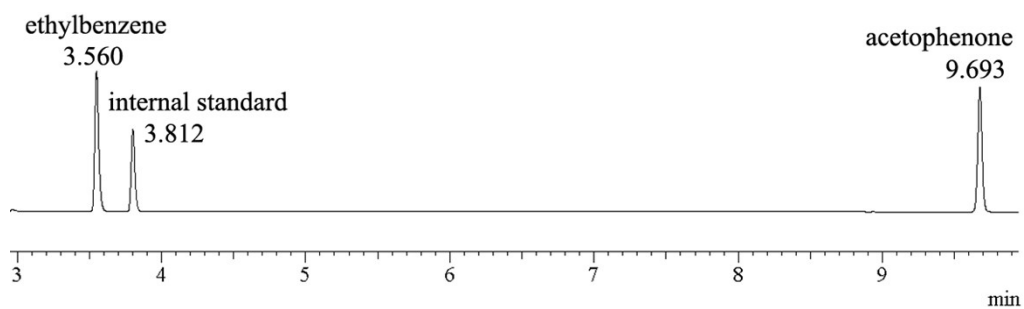
(h)



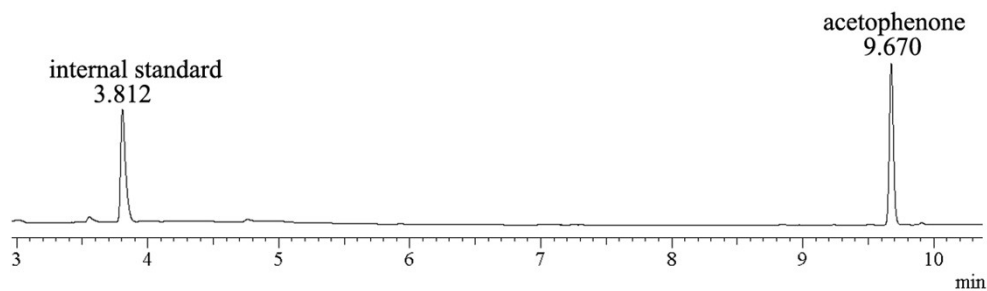
(i)



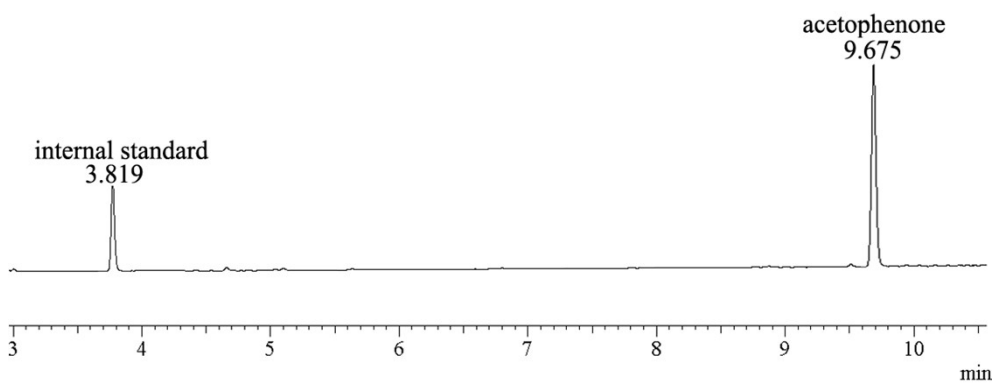
(j)



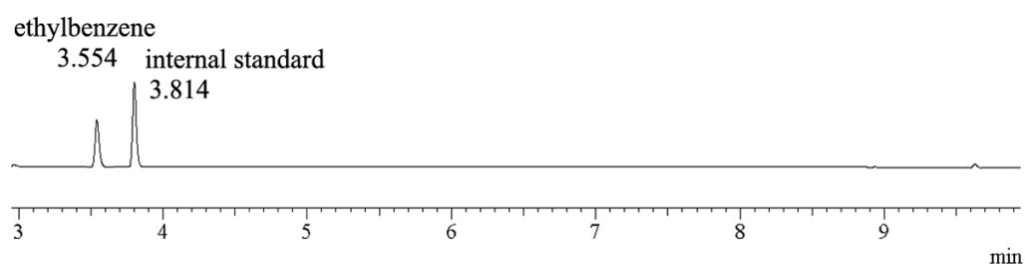
(k)



(l)



(m)



(n)

**Fig. S12.** (a) GC of the ethylbenzene oxidation experiment using catalyst **1** (1 mol%), internal standard, ethylbenzene and TBHP for 12 h. (b) GC of the ethylbenzene oxidation experiment using **2** (1 mol%), internal standard, ethylbenzene and TBHP for 12 h. (c) GC of the ethylbenzene oxidation experiment using **2** (1 mol%), internal standard, ethylbenzene and TBHP for 24 h. (d) GC of the ethylbenzene oxidation

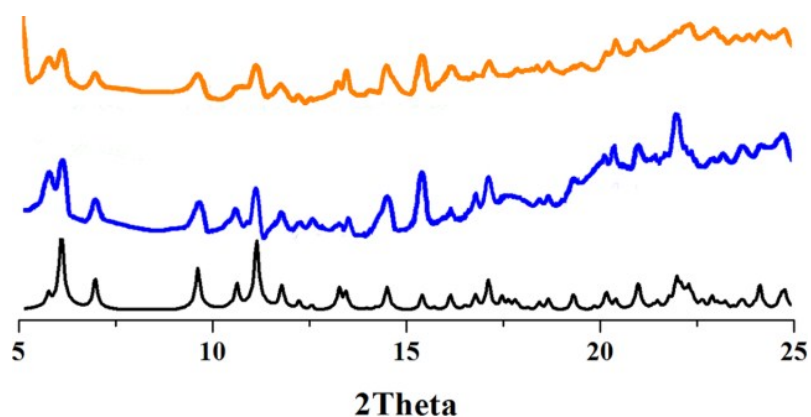
experiment using **1** (1 mol%), internal standard, ethylbenzene and TBHP for 2 h. (e) GC of the ethylbenzene oxidation experiment using **1** (1 mol%), internal standard, ethylbenzene and TBHP for 4 h. (f) GC of the ethylbenzene oxidation experiment using **1** (1 mol%), internal standard, ethylbenzene and TBHP for 6 h. (g) GC of the ethylbenzene oxidation experiment using **1** (1 mol%), internal standard, ethylbenzene and TBHP for 8 h. (h) GC of the ethylbenzene oxidation experiment using **1** (1 mol%), internal standard, ethylbenzene and TBHP for 10 h. (i) GC of the ethylbenzene oxidation experiment using **1** (5 mol%), internal standard, ethylbenzene and TBHP for 10 h. (j) GC of the ethylbenzene oxidation experiment using **1** (5 mol%), internal standard, ethylbenzene and TBHP for 12 h. (k) GC of the blank experiment using internal standard, ethylbenzene and TBHP for 12 h. (l) GC of the ethylbenzene oxidation experiment using H<sub>2</sub>TPPP, internal standard, ethylbenzene and TBHP for 12 h. (m) GC of the ethylbenzene oxidation experiment using **1** (1 mol%), internal standard, ethylbenzene and TBHP for 12 h after 5 cycles. (n) GC of the quenching experiment using **1** (1 mol%), internal standard, ethylbenzene, TBHP and *p*-benzoquinone (20 mol%) for 12 h.

**Table S3.** Catalytic activities of **1** and **2** in the oxidation of ethylbenzene <sup>a</sup>.

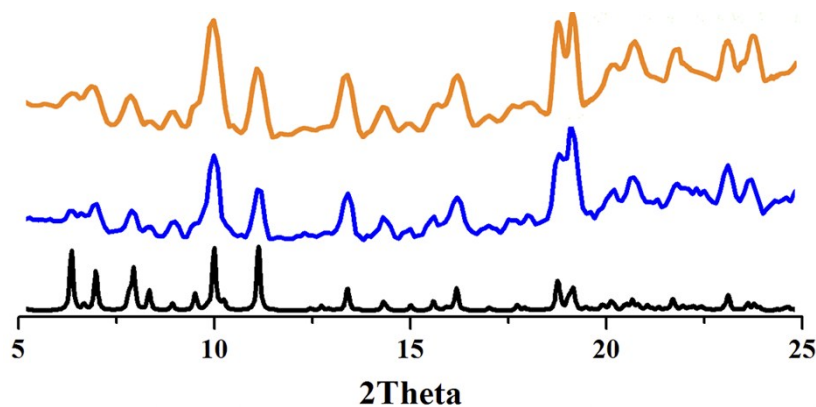
Entry	Catalyst	Reaction time (h)	Yield (%) <sup>b</sup>
1	<b>1</b>	12	>99
2	<b>2</b>	12	66
3	<b>2</b>	24	80
4	<b>1</b>	2	37
5	<b>1</b>	4	49
6	<b>1</b>	6	73
7	<b>1</b>	8	84
8	<b>1</b>	10	91
9	<b>1</b> <sup>c</sup>	10	88
10	<b>1</b> <sup>c</sup>	12	>99

11	<b>blank</b>	12	0
12	<b>H<sub>4</sub>TPPP</b>	12	60
13	<b>1<sup>d</sup></b>	12	90

<sup>a</sup>Reaction conditions: ethylbenzene (2.5 mmol), TBHP (1 mmol), catalyst (0.025 mmol), water (4 mL), 50 °C. <sup>b</sup>Isolated yield was calculated by GC. <sup>c</sup>5 mol% catalyst loading. <sup>d</sup>Fifth cycle.

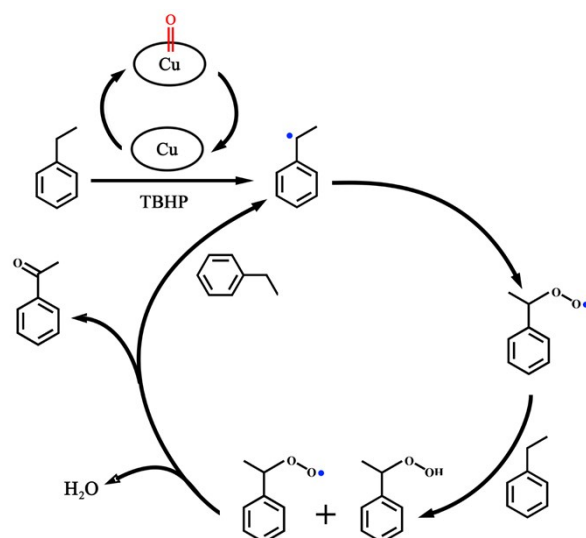


(a)



(b)

**Fig. S13.** (a) PXR D patterns of the simulated (black), the experimental (blue) and the ethylbenzene oxidation catalyzed by **1** (orange). (b) PXR D patterns of the simulated (black), the experimental (blue) and the ethylbenzene oxidation catalyzed by **2** (orange).



**Fig. S14.** Proposed mechanism of ethylbenzene oxidation using TBHP as oxidant.

**Photocatalytic reduction of  $K_2Cr_2O_7$  under visible light irradiation.** Hexavalent chromium Cr(VI) is extraordinary toxic in environment, which may cause inherited gene defects and cancer by inhalation.<sup>1</sup> While another oxidation state of chromium Cr(III) is harmless and essential trace metal in human nutrition.<sup>2</sup> Thus, reduction from Cr(VI) to Cr(III) is necessary and effective way to treat chromium-containing waste water.<sup>3</sup> In that case, selection of appropriate catalyst to reduce Cr(VI) to Cr(III) has gradually become research hotspot. In this study, we selected  $K_2Cr_2O_7$  as Cr(VI) source and isopropanol as hole scavenger. The photocatalytic reduction from Cr(VI) to Cr(III) with the use of catalysts **1** and **2** were monitored by UV-vis absorption spectra. Typically, the aqueous solution of  $K_2Cr_2O_7$  and crystalline catalysts were stirred in the dark for 30 minutes to achieve adsorption–desorption equilibrium. The photocatalytic reduction of Cr(VI) was performed under Xe lamp ( $\lambda > 420$  nm). As illustrated in Figure 3, after 3 hours of irradiation, the Cr(VI) ions were almost completely reduced to Cr(III) (95.4%) by catalyst **1** and the color of the solution changed from pale yellow to colorless (Fig. S13). For **2**, the reduction rate is slightly lower than that of **1** and only 45.6% of the  $K_2Cr_2O_7$  was reduced within the same time. Thus, catalyst **1** is much more effective than **2** during the reduction from Cr(VI) to Cr(III). Notably, the reduction reaction of Cr(VI) proceeds *via* a clear isosbestic point



at 315 nm, demonstrating that the redox reaction is proceeding smoothly without forming multiple products. It also should be pointed out that most of the Cr(VI) reduction occurred at low pH values or heating temperatures.<sup>4</sup> For the reduction reaction of Cr(VI) using catalysts **1** and **2**, a highly desired conversion rate was accomplished under the relatively mild conditions. Thereby, **1** and **2** are particularly promising economical efficient catalysts for the reduction of Cr(VI) ions.

On the basis of the experimental data discussed above, a tentative mechanism is proposed for the photoreduction activities of **1** and **2** toward Cr(VI). Under the visible light irradiation, porphyrin-based **1** and **2** was firstly excited to generate excited state electrons (Fig. S14).<sup>5</sup> Meanwhile, the isopropanol on the surface of **1** and **2** scavenge the holes produced by catalysts, and turns into reducing radicals.<sup>6</sup> Then it further transforms to harmless products such as CO<sub>2</sub> and H<sub>2</sub>O.<sup>7</sup> Apparently, this charge transfer process restrains the recombination of electrons and holes.<sup>8</sup> The electrons accumulated on catalysts **1** and **2** finally resulted in the implementation of reduction from Cr(VI) to Cr(III).<sup>9</sup>

- (1) J. L. Gardea-Torresdey, K. J. Tiemann, V. Armendariz, L. BessOberto, R. R. Chianelli, J. Rios, J. G. Parsons and G. Gamez, *J. Hazard. Mater.*, 2000, **80**, 175.
- (2) Y. Lin, W. Cai, X. Tian, X. Liu, G. Wang and C. Liang, *J. Mater. Chem.*, 2011, **21**, 991.
- (3) P. Miretzky and A. F. Cirelli, *J. Hazard. Mater.*, 2010, **180**, 1.
- (4) X.-L. He, Y.-P. Liu, K.-N. Gong, Z.-G. Han and X.-L. Zhai, *Inorg. Chem.*, 2015, **54**, 1215.
- (5) H. Wang, X. Yuan, Y. Wu, X. Chen, L. Leng and G. Zeng, *RSC Adv.*, 2015, **5**, 32531.
- (6) R. Liang, L. Shen, F. Jing, W. Wu, N. Qin, R. Lin and L. Wu, *Appl. Catal. B*, 2015, **162**, 245.
- (7) (a) B. Liu, J. Yang, G.-C. Yang and J.-F. Ma, *Inorg. Chem.*, 2013, **52**, 84; (b) L. Shen, S. Liang, W. Wu, R. Liang and L. Wu, *Dalton Trans.* 2013, **42**, 13649.
- (8) L. Shen, L. Huang, S. Liang, R. Liang, N. Qin and L. Wu, *RSC Adv.*, 2014, **4**,

2546.

(9) H. Wang, X. Yuan, Y. Wu, G. Zeng, X. Chen, L. Leng, Z. Wu, L. Jiang and H. Li,  
*J. Hazard. Mater.*, 2015, **286**, 187.

**Table S4.** Selected bond distances (Å) and angles (deg) for **1**.

Cu(1)-N(1)	1.985(6)	Cu(1)-N(2)	1.991(6)
Cu(1)-N(1) <sup>#4</sup>	1.991(6)	Cu(1)-N(2) <sup>#4</sup>	1.985(6)
Cu(2)-I(1)	2.5005(15)	Cu(2)-I(3) <sup>#1</sup>	2.6730(16)
Cu(2)-Cu(3)	2.7690(18)	Cu(2)-N(4)	2.190(8)
Cu(2)-N(5)	2.068(9)	Cu(3)-I(1)	2.6022(14)
Cu(3)-I(3) <sup>#1</sup>	2.6856(15)	Cu(3)-I(2)	2.5925(14)
Cu(3)-N(10) <sup>#2</sup>	2.075(7)	Cu(4)-I(2)	2.5461(14)
Cu(4)-I(3)	2.6235(15)	Cu(4)-N(8) <sup>#3</sup>	2.257(6)
Cu(4)-N(9) <sup>#3</sup>	2.050(6)	N(1)-Cu(1)-N(2) <sup>#4</sup>	90.1(2)
N(4)-Cu(2)-N(5)	78.2(3)	N(4)-Cu(2)-I(1)	116.5(2)
N(5)-Cu(2)-I(1)	123.3(3)	N(4)-Cu(2)-I(3) <sup>#1</sup>	119.5(2)
N(5)-Cu(2)-I(3) <sup>#1</sup>	95.9(3)	I(1)-Cu(2)-I(3) <sup>#1</sup>	116.24(5)
N(5)-Cu(2)-Cu(3)	140.2(3)	N(4)-Cu(2)-Cu(3)	139.9(2)
I(1)-Cu(2)-Cu(3)	58.92(4)	I(3) <sup>#1</sup> -Cu(2)-Cu(3)	59.11(4)
N(10) <sup>#2</sup> -Cu(3)-I(2)	106.6(2)	N(10) <sup>#2</sup> -Cu(3)-I(1)	101.2(2)
I(2)-Cu(3)-I(1)	116.95(5)	N(10) <sup>#2</sup> -Cu(3)-I(3) <sup>#1</sup>	106.7(2)
I(2)-Cu(3)-I(3) <sup>#1</sup>	111.76(5)	I(1)-Cu(3)-I(3) <sup>#1</sup>	112.39(5)
N(10) <sup>#2</sup> -Cu(3)-Cu(2)	127.4(2)	I(2)-Cu(3)-Cu(2)	125.93(5)
I(1)-Cu(3)-Cu(2)	55.39(4)	I(3) <sup>#1</sup> -Cu(3)-Cu(2)	58.66(4)
N(9) <sup>#3</sup> -Cu(4)-N(8) <sup>#3</sup>	77.8(2)	N(9) <sup>#3</sup> -Cu(4)-I(2)	138.7(2)
N(8) <sup>#3</sup> -Cu(4)-I(2)	99.29(16)	N(9) <sup>#3</sup> -Cu(4)-I(3)	105.2(2)
N(8) <sup>#3</sup> -Cu(4)-I(3)	109.87(18)	I(2)-Cu(4)-I(3)	114.17(5)

Symmetry transformations used to generate equivalent atoms: <sup>#1</sup> -x+1, y, -z+1/2; <sup>#2</sup> -x+1, y+2, -z+1/2; <sup>#3</sup> x, y+1, z; <sup>#4</sup> -x+3/2, -y-1/2, -z+1.

**Table S5.** Selected Bond Distances (Å) and Angles (deg) for **2**.

Ag(1)-N(1)	2.088(4)	Ag(1)-N(2)	2.076(5)
Ag(1)-N(3)	2.081(5)	Ag(1)-N(4)	2.077(5)
Ag(2)-N(18)	2.574(7)	Ag(2)-N(19)	2.247(7)
Ag(2)-N(10) <sup>#1</sup>	2.459(7)	Ag(2)-N(11) <sup>#1</sup>	2.303(7)
Ag(2)-O(1)	2.560(8)	N(2)-Ag(1)-N(4)	175.33(19)
N(2)-Ag(1)-N(3)	90.03(19)	N(4)-Ag(1)-N(3)	89.85(19)
N(2)-Ag(1)-N(1)	90.11(19)	N(4)-Ag(1)-N(1)	89.88(18)
N(19)-Ag(2)-N(11) <sup>#1</sup>	168.5(3)	N(19)-Ag(2)-N(10) <sup>#1</sup>	116.4(3)

N(11) <sup>#1</sup> -Ag(2)-N(10) <sup>#1</sup>	71.0(3)	N(19)-Ag(2)-O(1)	81.6(4)
N(11) <sup>#1</sup> -Ag(2)-O(1)	86.9(4)	N(10) <sup>#1</sup> -Ag(2)-O(1)	124.5(3)
N(19)-Ag(2)-N(18)	69.6(3)	N(11) <sup>#1</sup> -Ag(2)-N(18)	118.6(2)
N(10) <sup>#1</sup> -Ag(2)-N(18)	103.1(2)	O(1)-Ag(2)-N(18)	131.8(3)

Symmetry transformations used to generate equivalent atom: <sup>#1</sup>  $x, -y, z+1/2$ .

**Table S6.** Crystal data and structure refinements for **1** and **2**.

Compound	<b>1</b>	<b>2</b>
Formula	C <sub>78</sub> H <sub>58</sub> N <sub>22</sub> O <sub>2</sub> I <sub>6</sub> Cu <sub>7</sub>	C <sub>158</sub> H <sub>108</sub> Ag <sub>4</sub> N <sub>42</sub> O <sub>6</sub>
<i>Mr</i>	2541.69	3122.30
Crystal system	Monoclinic	Monoclinic
Space group	<i>C2/c</i>	<i>C2/c</i>
<i>a</i> (Å)	32.206(3)	22.3750(14)
<i>b</i> (Å)	8.8020(6)	17.7880(10)
<i>c</i> (Å)	30.440(3)	35.5640(19)
$\alpha$ (°)	90.00	90.00
$\beta$ (°)	108.120(11)	95.971(5)
$\gamma$ (°)	90.00	90.00
<i>V</i> (Å <sup>3</sup> )	8201.1(13)	14077.9(14)
<i>Z</i>	4	4
<i>D</i> <sub>calc</sub> (g cm <sup>-3</sup> )	2.059	1.473
<i>F</i> (000)	4868	6344
<i>R</i> <sub>int</sub>	0.0466	0.0615
GOF on <i>F</i> <sup>2</sup>	1.014	1.008
<i>R</i> <sub>1</sub> <sup>a</sup> [ <i>I</i> >2σ( <i>I</i> )]	0.0661	0.0845
<i>wR</i> <sub>2</sub> <sup>b</sup> (all data)	0.1791	0.2543

$$^a R_1 = \frac{\sum ||F_o| - |F_c||}{\sum |F_o|}, \quad ^b wR_2 = \left\{ \frac{\sum [w(F_o^2 - F_c^2)^2]}{\sum w(F_o^2)} \right\}^{1/2}.$$

**Table S7.** Crystal data and structure refinements for **2a** and **2b**.

Compound	<b>2a</b>	<b>2b</b>
Formula	C <sub>15</sub> H <sub>13</sub> N <sub>3</sub>	C <sub>15</sub> H <sub>12</sub> N <sub>3</sub> F
<i>Mr</i>	235.28	253.28
Crystal system	Monoclinic	Monoclinic
Space group	<i>P</i> 2 <sub>1</sub>	<i>P</i> <i>c</i>
<i>a</i> (Å)	7.9820(12)	5.6730(7)
<i>b</i> (Å)	5.766(2)	15.311(2)
<i>c</i> (Å)	13.788(2)	15.1600(19)
$\alpha$ (°)	90.00	90.00
$\beta$ (°)	100.341(2)	103.500(12)
$\gamma$ (°)	90.00	90.00
<i>V</i> (Å <sup>3</sup> )	624.3(3)	1280.4(3)
<i>Z</i>	2	4
<i>D</i> <sub>calc</sub> (g cm <sup>-3</sup> )	1.252	1.314
<i>F</i> (000)	248	528
<i>R</i> <sub>int</sub>	0.0652	0.0438
GOF on <i>F</i> <sup>2</sup>	1.046	1.025
<i>R</i> <sub>1</sub> <sup>a</sup> [ <i>I</i> > 2σ( <i>I</i> )]	0.0512	0.0564
<i>wR</i> <sub>2</sub> <sup>b</sup> (all data)	0.1308	0.1740

$$^a R_1 = \sum ||F_o| - |F_c|| / \sum |F_o|. \quad ^b wR_2 = \{ \sum [w(F_o^2 - F_c^2)^2] / \sum w(F_o^2)^2 \}^{1/2}.$$